Identifying the sources driving observed PM2.5 temporal variability over Halifax, Nova Scotia, during BORTAS-B

Atmos. Chem. Phys., 13, 7199–7213, 2013
www.atmos-chem-phys.net/13/7199/2013/
doi:10.5194/acp-13-7199-2013

Atmospheric Chemistry and Physics Open Access

Identifying the sources driving observed $PM_{2.5}$ temporal variability over Halifax, Nova Scotia, during BORTAS-B

M. D. Gibson[1], J. R. Pierce[2,3], D. Waugh[4], J. S. Kuchta[1], L. Chisholm[4], T. J. Duck[2], J. T. Hopper[1], S. Beauchamp[4], G. H. King[1], J. E. Franklin[2], W. R. Leaitch[5], A. J. Wheeler[6], Z. Li[7], G. A. Gagnon[8], and P. I. Palmer[9]

[1]Department of Process Engineering and Applied Science, Dalhousie University, Halifax, Nova Scotia, Canada
[2]Department of Physics and Atmospheric Science, Dalhousie University, Halifax, Nova Scotia, Canada
[3]Department of Atmospheric Science, Colorado State University, Fort Collins, Colorado, USA
[4]Environment Canada, Dartmouth, Nova Scotia, Canada
[5]Environment Canada, Toronto, Ontario, Canada
[6]Health Canada, Ottawa, Ontario, Canada
[7]College of Environmental Science and Engineering, Ocean University of China, Qingdao, China
[8]Department of Civil and Resources Engineering, Dalhousie University, Halifax, Nova Scotia, Canada
[9]School of GeoSciences, University of Edinburgh, Edinburgh, UK

Correspondence to: M. D. Gibson (mark.gibson@dal.ca)

Received: 23 January 2013 – Published in Atmos. Chem. Phys. Discuss.: 15 February 2013
Revised: 6 June 2013 – Accepted: 27 June 2013 – Published: 30 July 2013

Abstract. The source attribution of observed variability of total $PM_{2.5}$ concentrations over Halifax, Nova Scotia, was investigated between 11 July and 26 August 2011 using measurements of $PM_{2.5}$ mass and $PM_{2.5}$ chemical composition (black carbon, organic matter, anions, cations and 33 elements). This was part of the BORTAS-B (quantifying the impact of BOReal forest fires on Tropospheric oxidants using Aircraft and Satellites) experiment, which investigated the atmospheric chemistry and transport of seasonal boreal wildfire emissions over eastern Canada in 2011. The US EPA Positive Matrix Factorization (PMF) receptor model was used to determine the average mass (percentage) source contribution over the 45 days, which was estimated to be as follows: long-range transport (LRT) pollution: 1.75 $\mu g\,m^{-3}$ (47 %); LRT pollution marine mixture: 1.0 $\mu g\,m^{-3}$ (27.9 %); vehicles: 0.49 $\mu g\,m^{-3}$ (13.2 %); fugitive dust: 0.23 $\mu g\,m^{-3}$ (6.3 %); ship emissions: 0.13 $\mu g\,m^{-3}$ (3.4 %); and refinery: 0.081 $\mu g\,m^{-3}$ (2.2 %). The PMF model describes 87 % of the observed variability in total $PM_{2.5}$ mass (bias = 0.17 and RSME = 1.5 $\mu g\,m^{-3}$). The factor identifications are based on chemical markers, and they are supported by air mass back trajectory analysis and local wind direction. Biomass burning plumes, found by other surface and aircraft measurements, were not significant enough to be identified in this analysis. This paper presents the results of the PMF receptor modelling, providing valuable insight into the local and upwind sources impacting surface $PM_{2.5}$ in Halifax and a vital comparative data set for the other collocated ground-based observations of atmospheric composition made during BORTAS-B.

1 Introduction

Because of the importance of understanding the impact of North American boreal forest wildfires on Northern Hemisphere tropospheric chemistry, a multi-national project, led by the University of Edinburgh, was conducted out of Halifax, Nova Scotia, Canada, during the summer of 2011. The study aim was to quantify the impact of "BOReal forest fires on Tropospheric oxidants over the Atlantic using Aircraft and Satellites". Central to BORTAS-B was a measurement campaign with the UK Facility for Airborne Atmospheric Measurements (FAAM) BAe146 research aircraft (Parrington et al., 2012; Palmer et al., 2013). In addition, numerous satellite observations of trace pyrogenic gases were made (Tereszchuk et al., 2013).

A vital component of the BORTAS-B project was the Dalhousie University Ground Station (DGS) in Halifax. The DGS was established to determine the temporal variability of size-resolved particulate composition and gas species concentrations both in situ and through the atmospheric column. These measurements were used to help validate air quality forecast models used to guide the BAe146 aircraft toward wildfire plume outflows from within and exiting eastern Canada, to validate satellite surface and column composition observations over Halifax, to validate Lidar surface and column observations over Halifax, for identifying wildfire smoke plumes as they passed over or impacted the surface in Halifax and used for additional insight into the atmospheric chemistry prevalent during the BORTAS-B campaign. This paper presents the chemical speciation and mass concentration of atmospheric fine particulate matter composition less than, or equal to, a median aerodynamic diameter of 2.5 microns ($PM_{2.5}$). Receptor modelling of the $PM_{2.5}$ mass and chemical species was used in this paper to identify the local and upwind sources responsible for driving the observed temporal variability of $PM_{2.5}$ in Halifax sampled during the BORTAS-B mission.

2 Measurements

Figure 1 shows the geographical location of the DGS. The DGS is 65 m above sea level with the sampling inlets 15 m above ground level on the roof of the Sir James Dunn building, Dalhousie University, in the south end of Halifax (44°38′17.46″ N, 63°35′37.52″ W). The building is located in a residential area of Halifax away from strong local sources of $PM_{2.5}$. However, during the BORTAS-B study there were visible fugitive dust emissions caused by street landscaping and building renovations taking place in the vicinity of the DGS. This fugitive dust did not cause any operational issues with the instruments related to the receptor modelling of $PM_{2.5}$.

Twenty four (24) hour filter samples were collected at the BORTAS-B DGS from 20:00 UTC on 11 July 2011 to 20:00 UTC on 12 July 2011. Followed by uninterrupted 24 h filter samples taken from 20:00 UTC on 13 July 2011 to 20:00 UTC on 26 August 2011, resulting in a further 44 consecutive days of $PM_{2.5}$ samples, providing a total of 45 filter samples. The DGS sampling was scheduled for 20:00 UTC (16:00 Atlantic Standard Time) as this was the most practical time of day for the DGS research staff to synchronise multiple instrument 24 h sampling. Continuous measurements of $PM_{2.5}$ mass concentration, black carbon (BC), organic matter (OM) and meteorology were also collected over the same sampling period. The other collocated measurements at the DGS that are not featured in this paper are described in Palmer et al. (2013).

A Thermo 3500 ChemComb (Thermo Fisher Scientific Inc. Waltham, MA 02454, US) sampler operating at

Fig. 1. Location of the DGS used during BORTAS-B (source of maps: free within ArcGISv10).

$10\,L\,min^{-1}$ was loaded with a 47 mm diameter nylon filter for the collection of $PM_{2.5}$ anions (Br^-, Cl^-, NO_3^- and SO_4^{2-}), cations (Ca^{2+}, K^+, Na^+, NH_4^+ and Mg^{2+}) and water-soluble elements (As, Cr, Mn, P, Pb, Se and Sr). A sodium carbonate denuder was used in the ChemComb to scrub SO_2 from the sample air stream to prevent the formation of SO_4^{2-} artifacts on the nylon filter (Maykut et al., 2003; Dabek-Zlotorzynska et al., 2011). The flow rate of the ChemComb sampler was checked at the start and end of sampling with a NIST traceable Dry Cal Defender flow meter (accuracy of ±2 % of flow reading). A flow rate of ±20 % was deemed acceptable. In addition $PM_{2.5}$ were collected onto a 47 mm diameter, 2 µm Teflon filter (Whatman part #7592-104) for the analysis of mass and 33 elements using a Partisol 2025 dichotomous sampler (Dabek-Zlotorzynska et al., 2011). The Partisol flow rate was checked weekly with a Dry Cal Defender flow meter. The Partisol stopped sampling if the flow rate deviated by more than ±10 % of the set flow. Weekly internal and external leak checks were performed on the Partisol as per the manufacture's instructions, with no failures reported during the study.

No duplicate filter samples were taken during the study. Ten (10) % of the nylon and Teflon filters were field blanks

with an additional 5 % acting as laboratory blanks. Blank subtraction was conducted on all filter samples where required.

Assembly and disassembly of the ChemComb sampler and Partisol filter cassettes were conducted in a high-efficiency particle air (HEPA) cleaner hood.

The total $PM_{2.5}$ mass concentration was determined by gravimetric analysis of the Teflon filter sample at Alberta Innovates (Highway 16A and 75th Street, Vegreville, T9C 1T4 Alberta, Canada,) in accordance with US EPA protocol for the determination of ambient $PM_{2.5}$ mass concentration using filter-based sampling systems (USEPA, 1998).

The analysis of 33 elements (Ag, Al, As, Ba, Br, Ca, Cd, Ce, Cl, Co, Cr, Cs, Cu, Fe, In, K, Mg, Mn, Na, Ni, P, Pb, Rb, S, Sb, Se, Si, Sn, Sr, Ti, V, Zn and Zr) on the Teflon filter was conducted using a Thermo Fisher Scientific Quant'X energy dispersive x-ray fluorescence (ED-XRF) at RTI International (3040 Cornwallis Road, Building 7, RTP, NC 27709, USA). Due to low $PM_{2.5}$ sample mass, the following 14 elements measured by ED-XRF were not detected in any of the samples: Ag, Cd, Ce, Cs, In, P, Pb, Rb, Sb, Se, Sn, Sr, Ti and Zr.

The anions, cations and water-soluble elements were extracted from the nylon filters using 100 µL of HPLC grade isopropanol and 8 mL Type-1, 18 MΩ cm water followed by 30 min sonication. The anion and cation analysis was conducted using a Thermo Fisher Scientific, Dionex ICS-1000 ion chromatograph (Dionex Canada Ltd, RPO Maple Grove Village, Oakville, L6J 7P5 Ontario). Details of the Dionex instrument configuration and analysis protocol for the anion analysis is reported in Gibson et al. (2013). Cations were analysed using the Dionex ICS-1000 fitted with an IonPac CS-12 analytical column and guard column, 20 mM methanesulfonic acid eluent with an inject loop of 25 µL. The method used to determine the detection limit of the anions and cations is described in Gibson et al. (2013). Anions and cations not detected by ion chromatography in any of the samples included Br^-, F^-, HPO_4^{2-}, Mg^{2+} and NO_2^-. The water-soluble elements (As, Cr, Mn, P, Pb, Se, and Sr) extracted from the nylon filter were analysed using a Thermo X-Series II single quadrupole inductively coupled plasma-mass spectrometer (ICP-MS). A five-point standard curve of the isotope masses ^{75}As, ^{52}Cr, ^{55}Mn, ^{31}P, ^{208}Pb, ^{82}Se and ^{88}Sr were used for qualification and quantification. These elements were found to be above the detection limits in all samples.

Black carbon was estimated from continuous 1 min averages of light absorption at 880 nm using a Magee Scientific Corporation, AE42 aethalometer (1916A M. L. King Jr. Way, Berkeley, CA 94704, USA) (Lawless et al., 2004; Babu and Moorthy, 2002). The mass absorption conversion factor used was 16.6 (Hansen, 2005). The relative bias for the two monitors was determined by comparing the mean values over 5759 min of collocated readings. All readings of one monitor were multiplied by this factor to bring the means into agreement. The precision was then determined by calculating the absolute value of the difference between the monitors (after adjustment for the bias) divided by the sum of the readings for each minute as follows: $abs[(A-B)/(A+B)]$ (where A is the reading of the first monitor, and B is the reading of the second monitor adjusted by the bias). The median value for the 1 min readings was 0.18 (IQR 0.07–0.40). A precision and bias for 24 h was not possible as there were only three data points. The 1 min data points were averaged to match the 24 h $PM_{2.5}$ filter samples.

An Aerodyne Research, Inc., (Billerica, MA, US, 01821-3976) Aerosol Chemical Speciation Monitor (ACSM) (Ng et al., 2011) was operated by Environment Canada for the purposes of measuring continuous Cl^-, NH_4^+, NO_3^- OM and SO_4^{2-}, and at a temporal resolution of 30 min. The ACSM 30 min data points were averaged to match the 24 h $PM_{2.5}$ filter samples. Only the OM from the ACSM was used in the receptor modelling of the $PM_{2.5}$ as the Cl^-, NH_4^+, NO_3 and SO_4^{2-} from the nylon filter are recognised as the standard protocol for $PM_{2.5}$ speciation used in receptor modelling (Dabek-Zlotorzynska et al., 2011). Filter-based samples of OM were not available in this study, hence the use of the ACSM OM. The upper size cutoff (50 % transmittance) for the ACSM is ∼ 650 nm and the lower cut is 80–100 nm (Liu et al., 2007). While most of the organic (both primary and secondary) aerosol mass is at sizes smaller than 650 nm, it is possible that some of the mass between 650 nm and 2.5 µm was lost (Ng et al., 2011). Mass calibrations were performed before and after the experiment at Environment Canada in Toronto using nearly monodisperse particles of ammonium nitrate. The data completeness for the ACSM during BORTAS-B was 85 % (missing data between 2 August and 8 August). Stepwise regression (SR) was used to predict OM during the period of missing data. Twenty-one (21) $PM_{2.5}$ species variables and meteorological variables were used in the SR model. The significant OM predictor variables (p values, coefficient) used in the SR model were K ($p = 0.001$, 10.801), Ni ($p = 0.007$, −204.097), Zn ($p = 0003$, 121.884) and SO_4^{2-} ($p < 0.001$, 0.531). The SR constant was 0.157 with a model r^2 of 0.86. The artificial data generated for the 7 missing days of OM samples were used in the US EPA Positive Matrix Factorization (PMF) model. It was felt that this was superior to using the median OM concentration for the missing data period as suggested in the PMF user guide.

Meteorological data at the BORTAS-B DGS were collected every 15 min using a Davis Vantage Pro II weather station (Davis Instruments Corp. Hayward, California 94545, USA). The Davis Vantage Pro II weather sensors included wind speed, wind direction, temperature, pressure, solar radiation, UV radiation, relative humidity and precipitation. The meteorological data were integrated to match the 24 h filter-based sampling. The descriptive statistics of the meteorological variables that cover the $PM_{2.5}$ sampling period at

Table 1. Descriptive statistics for the daily averages of the meteorological variables obtained at the DGS during the $PM_{2.5}$ sampling period based upon 15 min average data.

	n	Mean	Std Dev	Min	25th Pctl	Median	75th Pctl	Max
Wind speed ($m\,s^{-1}$)	45	2.6	1.1	0.9	1.5	2.5	3.3	5.4
Temperature (°C)	45	18.9	1.9	15.1	17.5	19.2	20.3	24.2
Relative humidity (%)	45	84	9	64	78	84	91	97
Pressure (kPa)	45	100.2	0.4	99.1	99.9	100.2	100.6	101.1
Average wind vector: 238° ∼ SW								

the BORTAS-B DGS are provided in Table 1. The average wind vector coinciding with each 24 h $PM_{2.5}$ sample was determined using WRPLOT View (Lakes Environmental, Waterloo, Ontario, N2V 2A9, Canada).

In addition, Environment Canada used the meteorological data from Halifax International Airport (26.8 km distant at a heading of 012°) to provide an overview of meteorological conditions within the Halifax Regional Municipality during the 45 days of filter sampling at the BORTAS-B DGS. A climatology review of synoptic meteorology patterns over Maritime Canada indicates a general west-to-east progression of transport flow. The period of the filter-based measurements at the DGS in summer 2011 was influenced by numerous weak low-pressure systems during the first half of the sampling period (to 4 August). These systems, along with onshore moist southerly airflows provided extended periods with low-level clouds and occasional periods of rain, drizzle and fog. Low clouds tend to inhibit photochemistry and promote aqueous-phase production of SO_4^{2-}. Precipitation favours removal of particles from the atmosphere. Of the 45 sampling days, 13 had periods with sunny skies (6+ h). Ten of these days were in the latter portion of the sampling period, from 6 August onward, indicating limited photochemistry in the first portion of the sample period. Maximum 5 min averaged wind speed was significant (8.0 $m\,s^{-1}$ or more) on 7 days, with 20 August being the windiest. Rain with amounts > 0.2 mm occurred on 16 days, with 3 days (20 July, 2 August, 8 August) when amounts were greater than 20 mm. The 2 August rain event was due to a nearly stationary line of thunderstorms that developed over Halifax in the late afternoon. The line of thunderstorms did not move east of the area until the early hours of 3 August after providing 60+ mm of rain. A daily climatology review prepared by Environment Canada is presented in Table 2. These data were accessed via http://www.climate.weather.gc.ca/index_e.html.

3 Models

The HYbrid Single-Particle Lagrangian Integrated Trajectory (HYSPLIT) model was used to investigate the source regions of $PM_{2.5}$ measured at the DGS during BORTAS. The source of the data was the Global Data Assimilation System (GDAS) model accessed through the HYSPLIT web archive (http://ready.arl.noaa.gov/archives.php). Ten-day, 5-day and 2-day ensemble air mass back trajectories for the Halifax DGS during BORTAS were generated using the online HYSPLIT archive data (Draxler and Rolph, 2012; Rolph, 2012). Two trajectories were obtained for each 24 h sampling period (08:00 UTC and 20:00 UTC). The HYSPLIT default of 950 hPa (500 m) was chosen as the arrival height to avoid trajectories hitting the ground before they arrive at the DGS. The trajectory resolution was 1 h. It was found that a 2-day air mass trajectory identified the same upwind source region as a 10-day or 5-day trajectory. In addition, the visualisation of the ensemble trajectories was improved using 2-day trajectories. Therefore, 2-day ensemble air mass trajectories are presented.

The US EPA PMF receptor model v3 was used for source apportionment of the $PM_{2.5}$ sampled during BORTAS-B in Halifax. The PMF method has an extensive heritage, having been applied to many $PM_{2.5}$ source apportionment studies (Paatero, 1997; Paatero and Trapper, 1994; Martello et al., 2008; Jeong et al., 2011; Brown et al., 2007; Bari et al., 2009). Details of the PMF model are provided in Hopke (1991). A priori knowledge of sources, meteorology and the chemical markers present in the PMF factor profiles are used to identify the source, e.g. factors containing Ni and V are indicative of ship emissions (Jeong et al., 2011).

For the BORTAS-B $PM_{2.5}$ mass and species data the uncertainty was set to the PMF default of 20 %. For all model base runs, twenty random initialisations were conducted. Once the base run was completed the scatter plots and times series of the modelled and observed $PM_{2.5}$ species were scrutinised with outliers being investigated. The normality of the model-scaled residuals for each $PM_{2.5}$ species was also scrutinised. Any $PM_{2.5}$ species-scaled residuals found to be ± 3 from zero were investigated further for poor model fit. Two checks on model performance were then made: bootstrapping and the PMF FPeak function. To fine tune the model the FPeak function within PMF was used to robustly minimise the effect of outliers. However, FPeak failed to improve the model and so was set to zero. The G-Space function was used to also check for model performance, with no issues found with any of the species bi-plots. Once confidence in the model was achieved, the PMF factor profiles were allocated

Table 2. Daily meteorological summary covering the filter sampling period 11 July 2011 to 25 August 2011 from Halifax International Airport.

	Meteorological Data Summary Key
	Dates in bold italics indicate a date with significant sunshine (≥ 6 h).
	Dates in bold indicate a date with precipitation > 0.2 mm.
	Descriptive text in bold highlights a significant meteorological feature.
	Wind speed ($m\,s^{-1}$)
	Temperature (°C)
	Time UTC
11 Jul	Cloudy with midday and afternoon sunshine. Wind S to SW 3 became SW 6–8 14:00. High 25.
12 Jul	Overnight fog then rain or showers to 18:00. Wind S 6–7 then light in eve. High 17.
13 Jul	Fog to 11:00 then mostly cloudy. Wind N at 6–8. High 23.
14 Jul	Clear to start then cloudy before sunrise with rain by 21.00. Wind N 6–8. High 13.
15 Jul	Rain ended at sunrise then cloudy then rain from 23:59. Wind **N 6–11**. High 19.
16 Jul	Mostly cloudy with wind **NW 8** then dropped off by 23:00. High 20.
17 Jul	Mostly clear to 12:00 then mostly cloudy. Wind SW 6. **High 30**.
18 Jul	Mostly cloudy with a shower at noon. Clearing in evening. Wind SW 4–6. High 25.
19 Jul	Fog overnight then mostly cloudy with scattered showers. Wind SW 3. High 26.
20 Jul	Mainly clear to 21:00 then cloudy. Wind W 3 except SW **8** at 21:00 then SW 6–7. High 27.
21 Jul	Cloudy then Rain Fog and a Thundershower in late evening. Wind SW 6–8 **except 8** late evening. High 28.
22 Jul	Fog to 14:00 then mostly cloudy. Wind W 3 then light then SE 6 then N 4. High 28.
23 Jul	Fog to 14:00 then mostly cloudy, 20:00 shower then Fog. Wind light N then S 4–6.
24 Jul	Clear early morning then mostly cloudy then clear in evening. Wind NW–N 4–6 then light in the evening. High 23.
25 Jul	**Clear. Wind light.** Then S 4 from midafternoon. High 24.
26 Jul	Clear at first then mostly cloudy to cloudy with fog in the evening. Wind SE 4–6 light in the eve.
27 Jul	Fog to midday then cloud with suppertime showers. Wind SE 3. High 19.
28 Jul	Fog early then mostly cloudy. Wind NW–N 4. High 20.
29 Jul	Clear then mostly cloudy after 09:00. Wind light then SW 6–7 after midday. High 23.
30 Jul	Fog to morning then mostly rain through day – drizzle in the evening. Wind S-SE 4-6 became N 7 late eve. High 18.
31 Jul	Mostly cloudy except clear midday and then in evening. Wind NW 4–6. High 25.
Aug 1	Clear to sunrise then mostly cloudy to sundown. Wind light then SE 4 after noontime. High 24.
2 Aug	Fog then cloudy. Thunderstorms from midafternoon through evening. Wind SE 6–8. High 22.
3 Aug	Thunderstorms and rain until 07:00 then cloudy, showers in the morning. Wind ESE 6–8. High 17.
4 Aug	Cloudy, showers to midday. Wind NE 4–6. High 18.
5 Aug	Mostly cloudy to late evening. Wind N 4–7. High 19.
6 Aug	Fog overnight then mainly clear after 12:00. Wind NW 3 then light in evening. High 24.
7 Aug	Cloudy to late morning then some sun. Rain late evening. Wind S–SE 3. High 25.
8 Aug	Fog, drizzle and showers then rain by midday ended in the evening. Wind S–SE 4–6. High 19.
9 Aug	Fog overnight then cloudy with evening drizzle. Wind N 6–8 then light in evening. High 20.
10 Aug	Fog and drizzle to midmorning then cloudy. Showers in the evening. Wind SE 6 occasionally **8**. **High 16**
11 Aug	Fog then morning drizzle then cloudy with some late day sun. Wind SE 4–6. High 19.
12 Aug	Some early morning fog otherwise clear. Wind W 1–3 then SE 4 later afternoon. High 24.
13 Aug	**Clear**. Light except NW 4 midday hours. High 25.
14 Aug	Clear then mostly cloudy in the afternoon. Wind SW 4–6. High 26.
15 Aug	Fog then mostly cloudy with eve showers and rain. Wind SE 3–4. High 23.
16 Aug	Rain and drizzle. Clear to supper. Then cloudy with late drizzle. Wind SE 6 then to **8 in the afternoon**.
17 Aug	Showers and drizzle end overnight. Then clear by 13:00. Wind NW 6. High 24.
18 Aug	**Clear**. Wind light SW then S–SW 6–8. High 25.
19 Aug	Fog patches to sunrise then cloudy but clear by noon. Wind SW 3–4 the S 6 from midafternoon. High 25.
20 Aug	Fog patches overnight then mostly cloudy with sunny periods. Clear late eve. Wind SW–S 4-7. High 26.
21 Aug	Fog overnight. Then clear in the am then mostly cloudy. Wind S–SW 10 becoming 6–7 at 16:00.
22 Aug	Cloudy with overnight fog. Rain showers from midafternoon onward. Wind S 6–8 **with G 11**. High 22.
23 Aug	Mainly clear. Wind NW 4–6 becoming W 3–4 late in the day. High 23.
24 Aug	Clear then mostly cloudy from 15:00 onwards. Wind W 3 but SSW 6–8 in afternoon evening. High 24.
25 Aug	Few sunrise fog patches. Otherwise clear to early afternoon then cloudy. Wind S 3–4 then **SSW 8–11** dropping to SSW 6 in evening. High 25. Remnants of TS. Irene forecast for Sunday, 28.
Precipitation summary: 17 days with more than 0.2 mm. Heavy precipitation days > 20 mm: 20 Jul, 2 Aug and 8 Aug.	

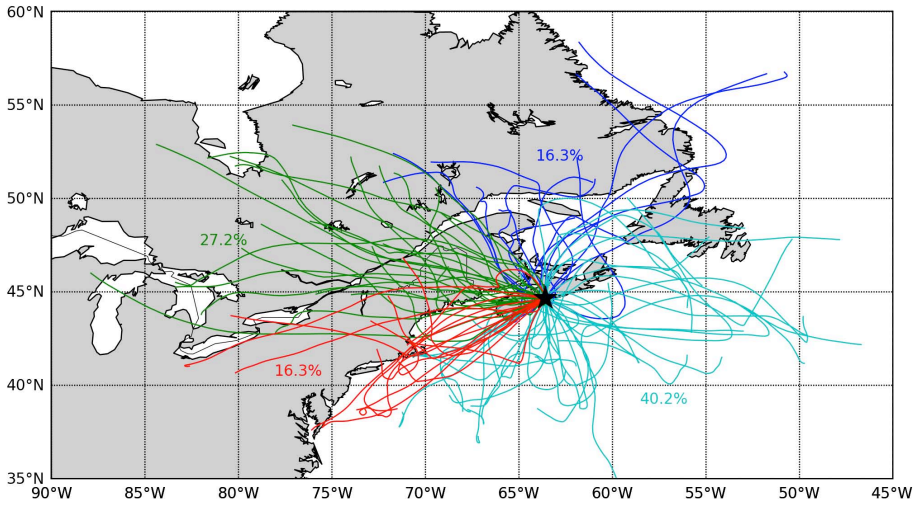

Fig. 2. Map of ensemble HYSPLIT 2-day air mass back trajectories between 11 July 2011 and 25 August 2011. Trajectories were initialised twice per day at 08:00 UTC and 20:00 UTC with an arrival height of 500 m. Colours denote upwind source region (cyan = marine; red = SW; green = WN; and blue = N).

a "source name" based upon the factor loadings of the key chemical markers present.

Chemical markers are used to help identify sources within the PMF source profiles; e.g. biomass burning has a number of characteristic chemical markers, e.g. K, BC and levoglucosan (1,6-anhydro-β-D-glucopyranose) (Bergauff et al., 2010; Ward et al., 2012; Jeong et al., 2008). Potassium is a good marker of long-range wildfire smoke plumes as it is conserved from source to receptor (Ward et al., 2012). Levoglucosan is also a good marker for local biomass burning, but it is readily oxidised to 17 % of its original primary mass after 3.5 h of exposure to hydroxyl radicals (OH) (Hennigan et al., 2011), which may reduce its ability to identify LRT of biomass burning. However, internally mixed levoglucosan may not be oxidised, being protected by the outer layer of the particulate, and so may still be useful as a marker of LRT boreal wildfire burning (Hennigan et al., 2011). Robust chemical markers of ship emissions include SO_4^{2-}, V, Ni and BC (Hobbs et al., 2000; Isakson et al., 2001; Zhao et al., 2013). V / Ni ratios originating from heavy fuel oil (HFO) used in ships range from 1.9 to 6.5 (Zhao et al., 2013). The sulphur content of HFO is currently between 1.0 % and 3.5 %, and during combustion produces particulate SO_4 (Lack et al., 2011). Ship emissions also contain large quantities of BC particulate (Lack and Corbett, 2012). Unambiguous markers of fugitive surficial dust include Fe, Al, Ca and Si (Jeong et al., 2011; Martello et al., 2008; Gugamsetty et al., 2012). Primary sea salt markers include Na^+, Cl^-, Mg^{2+} and Ca^{2+} (Gibson et al., 2009), and Na^+, Mg^{2+}, Ca^{2+} and NO_3^- for aged marine secondary aerosol (Jeong et al., 2011; Gibson et al., 2009). Nitrate, NH_4^+ and SO_4^{2-} are markers of long-range secondary inorganic PM produced by the gas-to-particle conversion of the pre-cursor gases ammonia (NH_3), NO_2 and SO_2 (Yin and Harrison, 2008; Gibson et al., 2009). Chemical markers for vehicular emissions include BC, Br, Fe, Mn and Sb (Larson et al., 2004; Huang et al., 1994). Barium, Cu, Sb and Fe are markers for vehicle brake wear (Harrison et al., 2011; Bukowiecki et al., 2010; Chen et al., 2007), and Cd and Zn are markers for vehicle tyre wear (Bukowiecki et al., 2010; Olajire and Ayodele, 1997; Chen et al., 2007). Diesel emissions have been previously characterised by high PMF loading of $PM_{2.5}$ mass and BC (Martello et al., 2008; Chen et al., 2007). Selenium is often used as a good marker for coal combustion, with Pb acting as a good marker for industrial emissions (Chow et al., 2004; Jeong et al., 2011). The source chemical profiles contained in the US EPA Speciate database provide additional evidence to identify source chemical markers in PMF chemical species factor profiles (Ward et al., 2012; Jaeckels et al., 2007).

The sum of the masses associated with the apportioned sources obtained from PMF were then compared with the original total $PM_{2.5}$ mass. The bias of the PMF model is calculated as $(A - T)/T$, where A is the PMF $PM_{2.5}$ mass concentration and T is observed $PM_{2.5}$ mass concentration over the 44 days of sampling. The root-mean-square error (RMSE) (Laupsa et al., 2009) will be used to determine the accuracy of the PMF model:

$$\mathrm{RMSE} = \sqrt{\frac{1}{n}\sum_{i=1}^{n}\left(\hat{y} - y_i\right)^2}, \quad (1)$$

where $\hat{y}$ represents PMF model total $PM_{2.5}$ mass concentration and y_i represents observed total $PM_{2.5}$ mass concentration, with units expressed in $\mu g\,m^{-3}$.

4 Results and discussion

4.1 HYSPLIT cluster analysis

The HYSPLIT 2-day ensemble air mass back trajectories are provided in Fig. 2, with the mean location of the trajectory over the 2-day travel time used to group the trajectories into four clusters: (1) N (315° to 45°), (2) marine (45° to 235°), (3) SW (235° to 265°), and (4) W–NW (265° to 315°). These clusters were chosen to reflect known source regions in central Canada, Atlantic Canada and the north-eastern United States; e.g. trajectory clusters coloured cyan are clearly under the influence of marine aerosol, and the SW cluster (red) covers the Ohio valley, the interstate-95 corridor and other source regions in the NE US (Jeong et al., 2011; Dabek-Zlotorzynska et al., 2011). The NW cluster (green) covers the Windsor–Québec corridor, which is the population and industrial core of central Canada and, as such, a major source region of secondary inorganic species and secondary OM (Jeong et al., 2011; Dabek-Zlotorzynska et al., 2011). The N cluster (blue) is a region of low anthropogenic emissions and should represent fairly clean air parcels impacting Halifax. Figure 2 shows that 40 % of the air masses entering Halifax during the BORTAS-B $PM_{2.5}$ sampling campaign originated from the marine sector: 16 % from the SW (NE US), 27 % from the WNW (Windsor-Quebec source region) and 16 % from the N. Figure 3 shows that air mass back trajectories from all four clusters have a high likelihood that the trajectory profiles were in the boundary layer during the previous 48 h. Our analysis also showed that over 80 % of the back trajectories were below 1.5 km for the entire 48 h. The profiles from the N (blue) show the highest probability of air subsiding from the free troposphere; however, it was anticipated that these profiles would be associated with clean air regardless of the altitude of the back trajectories. As expected, the marine cluster mostly originated from the boundary layer (Holzinger et al., 2007). Of the two potentially polluted clusters shown in Fig. 3, the SW cluster and WNW cluster appear to be mainly associated with boundary layer flow.

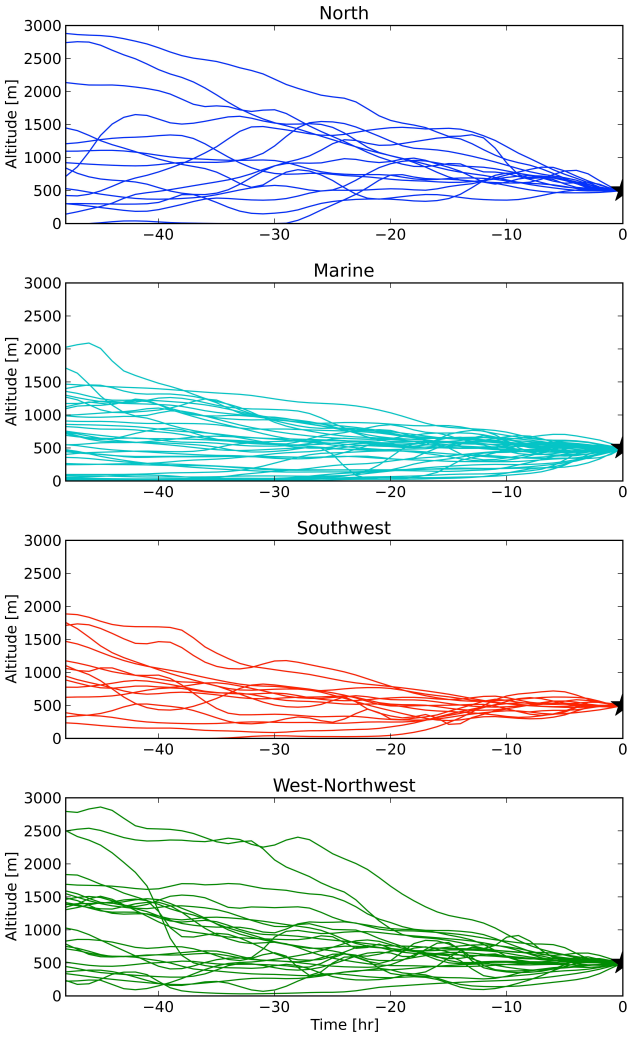

Fig. 3. HYSPLIT 2-day air mass back trajectory vertical profiles initialised twice per day at 08:00 UTC and 20:00 UTC.

4.2 Descriptive statistics

Table 3 shows the descriptive statistics for the $PM_{2.5}$ species sampled during BORTAS-B. The median $PM_{2.5}$ concentration is 3.9 µg m^{-3}, which is considerably lower than historical (2006–2008) summertime values (median 9.0 µg m^{-3}) measured at the National Air Pollution Surveillance (NAPS) station in downtown Halifax and reported by Jeong et al. (2011). The difference between these two values might be due to greater vehicle density in the downtown core of Halifax compared to the DGS that is located in the more residential south end of Halifax. Unfortunately, the Federal Government $PM_{2.5}$ monitoring in downtown Halifax during BORTAS-B was too sparse to make any direct comparison with our data possible. The BORTAS-B $PM_{2.5}$ median is also considerably lower than summertime median $PM_{2.5}$ concentrations found in Toronto (12 µg m^{-3}) and Windsor, Canada (15 µg m^{-3}) (Jeong et al., 2011), which can be attributed to the significantly lower population, vehicle and industrial density in Halifax in comparison to these other Canadian cities. In addition, with reference to Table 2, precipitation amounts > 0.2 mm occurred on 16 days, with two days (2 August and 8 August) when amounts were greater than 20 mm. The significant precipitation occurring during roughly half of the sampling period helps explain the reduced average $PM_{2.5}$ concentrations observed during BORTAS-B when compared with previous years. Despite the low $PM_{2.5}$ sample mass, the key chemical species needed to conduct PMF modelling were above the limit of detection (LOD).

Table 3. Descriptive statistics of $PM_{2.5}$ mass ($\mu g\,m^{-3}$) and species mass ($\mu g\,m^{-3}$) used in the PMF analysis.

	n	Mean	Std	Min	25th Pctl	Median	75th Pctl	Max	Data completeness %	LOD
Total $PM_{2.5}$	45	4.5	3.4	0.08	2.1	3.9	5.6	13.7	100	0.04
Black carbon	45	0.41	0.21	0.12	0.26	0.39	0.52	1.03	100	0.01
Organic matter	45	1.05	0.72	0.18	0.48	0.77	1.50	2.77	85	0.10
Al	45	0.020	0.016	0.0091	0.0091	0.011	0.028	0.086	100	0.0070
As	45	0.0010	0.00076	0.00015	0.00054	0.00087	0.00114	0.0040	100	0.00010
Ba	45	0.0063	0.0020	0.0031	0.0056	0.0056	0.0063	0.0163	100	0.0026
Br	45	0.0015	0.00079	0.00095	0.0010	0.0013	0.0017	0.0047	100	0.00086
Ca	45	0.017	0.019	0.0021	0.0089	0.014	0.016	0.13	100	0.0015
Cl	45	0.046	0.070	0.0019	0.0042	0.011	0.045	0.32	100	0.0015
Cr	45	0.0022	0.00079	0.00035	0.0017	0.0020	0.0027	0.0040	100	0.00030
Cu	45	0.0013	0.00050	0.00062	0.00095	0.0013	0.0015	0.0028	100	0.00060
Fe	45	0.0240	0.0200	0.00110	0.0110	0.0180	0.0280	0.0970	100	0.00065
K	45	0.023	0.019	0.0017	0.011	0.018	0.027	0.11	100	0.0010
Mg	45	0.017	0.018	0.0039	0.0060	0.014	0.020	0.11	100	0.0035
Mn	45	0.00031	0.00029	0.00010	0.00010	0.00025	0.00036	0.0017	100	0.00005
Na	45	0.11	0.12	0.0089	0.037	0.090	0.13	0.73	100	0.00081
NH_4^+	45	0.23	0.27	0.0030	0.066	0.15	0.27	1.45	100	0.0010
Ni	45	0.0011	0.00078	0.00044	0.00046	0.00070	0.0015	0.0037	100	0.00016
NO_3^-	45	0.093	0.10	0.0074	0.042	0.067	0.10	0.64	100	0.0030
P	45	0.0020	0.0017	0.000040	0.00079	0.0015	0.0023	0.0081	100	0.000010
Pb	45	0.00037	0.00035	0.000060	0.00014	0.00027	0.00050	0.0017	100	0.000032
S	45	0.39	0.34	0.0022	0.18	0.29	0.42	1.81	100	0.0009
Se	45	0.00019	0.00027	0.000080	0.000080	0.000080	0.000080	0.0015	100	0.00008
Si	45	0.042	0.048	0.0044	0.014	0.030	0.056	0.29	100	0.0036
SO_4^{2-}	45	0.78	0.97	0.14	0.26	0.47	0.70	5.59	100	0.070
Sr	45	0.00055	0.00034	0.000010	0.00041	0.00049	0.00060	0.0021	100	0.000010
V	45	0.0033	0.0027	0.0016	0.0016	0.0026	0.0038	0.017	100	0.00092
Zn	45	0.0023	0.0017	0.00070	0.0012	0.0019	0.0030	0.0089	100	0.00051

4.3 $PM_{2.5}$ composition

Figures 4–7 shows time series of daily major, macro, minor and trace $PM_{2.5}$ components together with the total $PM_{2.5}$ mass concentration. The main contributing species seen during the relatively low $PM_{2.5}$ concentrations observed between 13 July and 15 July were Na and Cl (indicative of sea salt) as well as some OM and BC from local combustion emissions (Chow et al., 2004; Dabek-Zlotorzynska et al., 2011). The air mass back trajectories during this low $PM_{2.5}$ mass period were from the north, a region of low primary and secondary $PM_{2.5}$ emission, thus providing evidence to explain the low concentrations experienced on 13 July and 15 July. Between 16 July and 24 July there was a $PM_{2.5}$ episode as shown in Fig. 4. Figures 4 and 5 show that the dominant species during this period were BC, NH_4^+, S, SO_4^{2-}, NO_3^- and OM with input from Se and Pb, as shown in Fig. 7. The presence of Se indicates input from coal-fired power stations and Pb being a marker of industry, the likely source region being the NE US airshed (Martello et al., 2008). The elevated Cl and Na provide evidence that the air mass also crossed the ocean before reaching Halifax. This is corroborated by air mass trajectories over this period which show that the airflow was from the SW and eastern seaboard of the US, and this will be discussed later with the PMF results. With reference to Table 2, there was a thunderstorm on 19 July that likely explains the sudden reduction in $PM_{2.5}$ concentration due to aerosol "wash-out" on this day compared to the preceding and following days.

Figure 6 shows a fugitive dust event on 23 August, which is characterised by elevated concentrations of Al, Ca, Fe, K and Si, which are known crustal elements. The weather on 23 August was dry, warm (23 °C), with clear skies and accompanied by high winds (3–4 $m\,s^{-1}$) throughout the 24 h period, conditions favourable to the re-suspension of surficial dust. There was also considerable street landscaping and exterior building restoration taking place on this day, again providing supportive evidence for fugitive dust suspension. Figure 7 shows elevated Ba and Cu on 23 August, which are known markers of brake wear contamination of resuspended road dust and urban soils (Harrison et al., 2011; Bukowiecki et al., 2010). Therefore, brake wear components are probably an additional component of the elevated fugitive dust seen on 23 August. From Fig. 7 it can be seen that there were elevated concentrations of As, Ba, Cu and Zn on 31 July and 13 August, which are known markers for vehicles

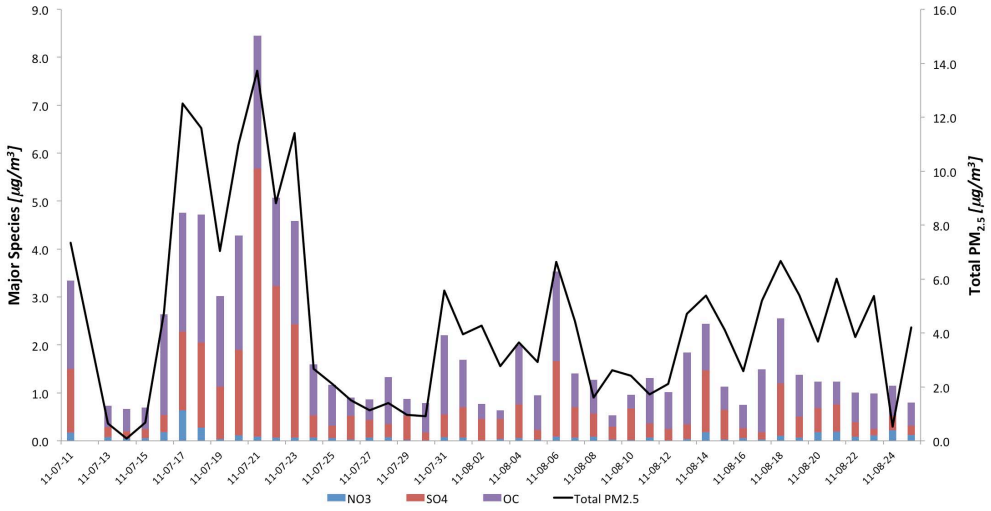

Fig. 4. Time series of total $PM_{2.5}$ mass and major species concentration.

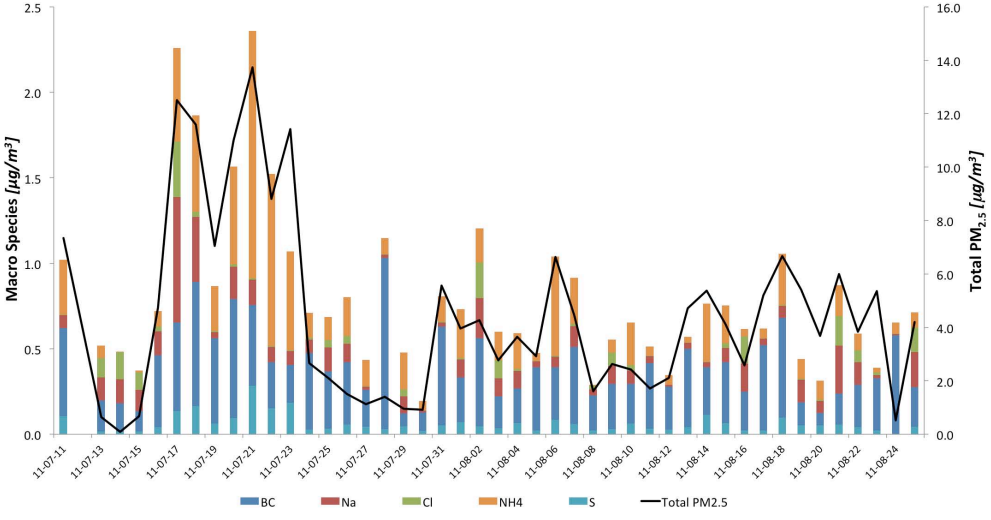

Fig. 5. Time series of total $PM_{2.5}$ mass and macro species concentration.

(Harrison et al., 2011; Bukowiecki et al., 2010). The wind direction on these two days was from the NW, which is in line with the 102 Highway and other major and minor roads upwind of the sampling site (again, this will be shown with the PMF results). In addition, on 31 July and 13 August it was dry, with winds between 4–6 m s^{-1} and 4 m s^{-1} respectively: conditions that favour transport and re-suspension of vehicle emissions, tyre debris and brake wear, which are the probable sources of these elevated metal concentrations seen on 31 July and 13 August. Figure 7 also shows elevated Ni, V and SO_4^{2-} on 10 August. The local wind direction on this day was from the SE and aligned with Halifax harbour. The wind direction coincident with the harbour, together with the presence of elevated Ni, V and SO_4^{2-}, suggest ship emissions as the probable source contributing to the $PM_{2.5}$ mass on this day (Zhao et al., 2013).

4.4 PMF receptor modelling

The number of factors (sources) that PMF could apportion were explored in an iterative process from 5 factor profiles through to 15 factor profiles. The number of factors chosen was based on the high factor loadings of key chemical markers, the ensemble HYSPLIT trajectory clusters (Fig. 2), wind roses analysis and a priori knowledge of known sources impacting Halifax. The seven factors chosen were LRT pollution (LRTP), LRT pollution marine mixture (LRTPMM), refinery, ship emissions, vehicles, fugitive dust and sea salt, which were anticipated by the individual chemical markers related to these sources as discussed in section 4.3. High factor loadings of NH_4^+, OM, $PM_{2.5}$ and SO_4^{2-}, S and were used to identify LRTP. High factor loadings of Na^+, NO_3^- and OM were used to identify LRTPMM. The LRTPMM is likely a

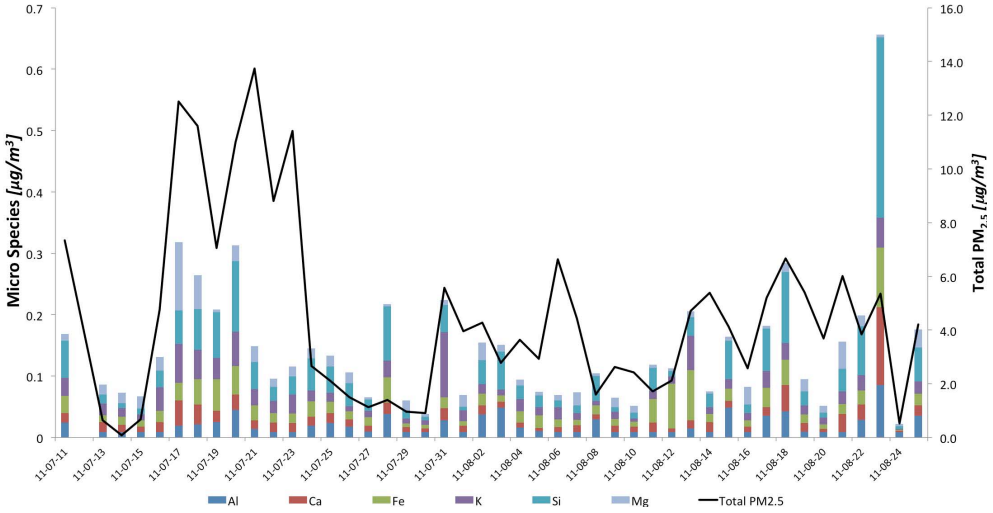

Fig. 6. Time series of total $PM_{2.5}$ mass and micro species concentration

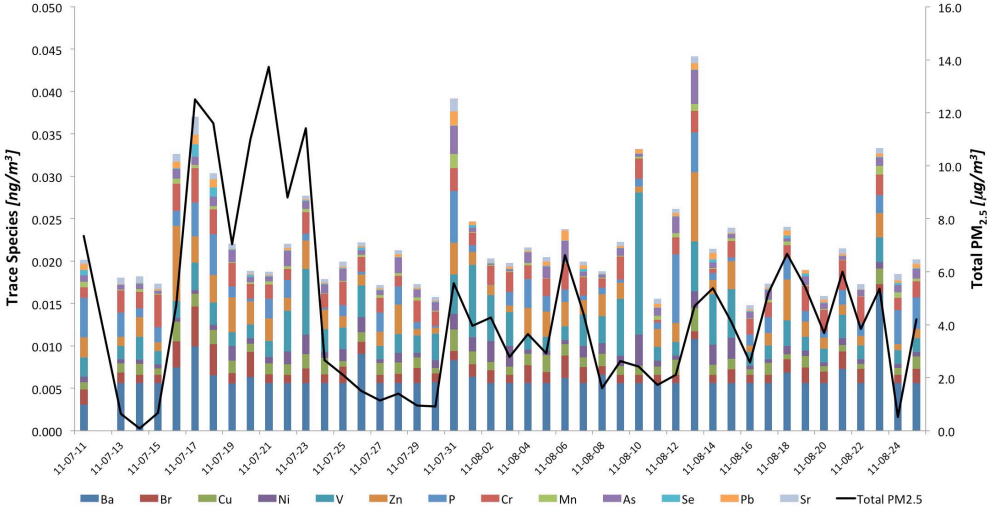

Fig. 7. Time series of total $PM_{2.5}$ mass and trace species concentration

mixture of aerosol pollution outflow from the NE US and sea salt that has undergone Cl^- loss via reactions with acidic aerosol (Gibson et al., 2009; Leaitch et al., 1996; Calvert et al., 1985). The presence of NO_3^- in the LRTPMM could also be attributed to night-time reactions of NO_2 with O_3, with NO_3^- also reacting with sea salt to remove Cl^- (Finlayson-Pitts and Pitts, 1999; Calvert et al., 1985). The refinery factor was identified by the presence of Cr, Cu, Pb, V and Zn (Jeong et al., 2011). Ship emissions were identified by the high factor loadings of BC, Ni, SO_4^{2-} and V (Zhao et al., 2013). Vehicles were identified by the high factor loadings of Ba, BC, Br, Cu, OM and Zn (Gietl et al., 2010). It was not possible with this data set to split the vehicle factors into gasoline or diesel emissions, brakes or tyre wear sources. Fugitive dust was identified by high factor loadings for Al, Ca, K, Fe and Si (Jeong et al., 2011). Sea salt was identified from the high factor loadings for Cl and Na, 88 % and 55 % respectively, which is the same ratio as found in sea water (Gibson et al., 2009). Figure 8 shows the source profiles for the seven factors identified within the PMF model. Although sea salt was observed in all PMF factor iterations, 5 through 15, the mass contribution was so low that PMF failed to apportion mass to any of the PMF model runs. This is perhaps not surprising given the very low $PM_{2.5}$ mass observed during BORTAS-B and the fact that sea salt PM are mostly associated with the coarse size fraction. However, there was evidence of a contribution of aged marine aerosol (as indicated by the presence of Na and NO_3^- markers) to the LRTPMM source coincident with airflow from the NE US and crossing the ocean en route to Halifax (Leaitch et al., 1996). Therefore, the PMF receptor model apportioned six $PM_{2.5}$ sources. Figure 9 presents

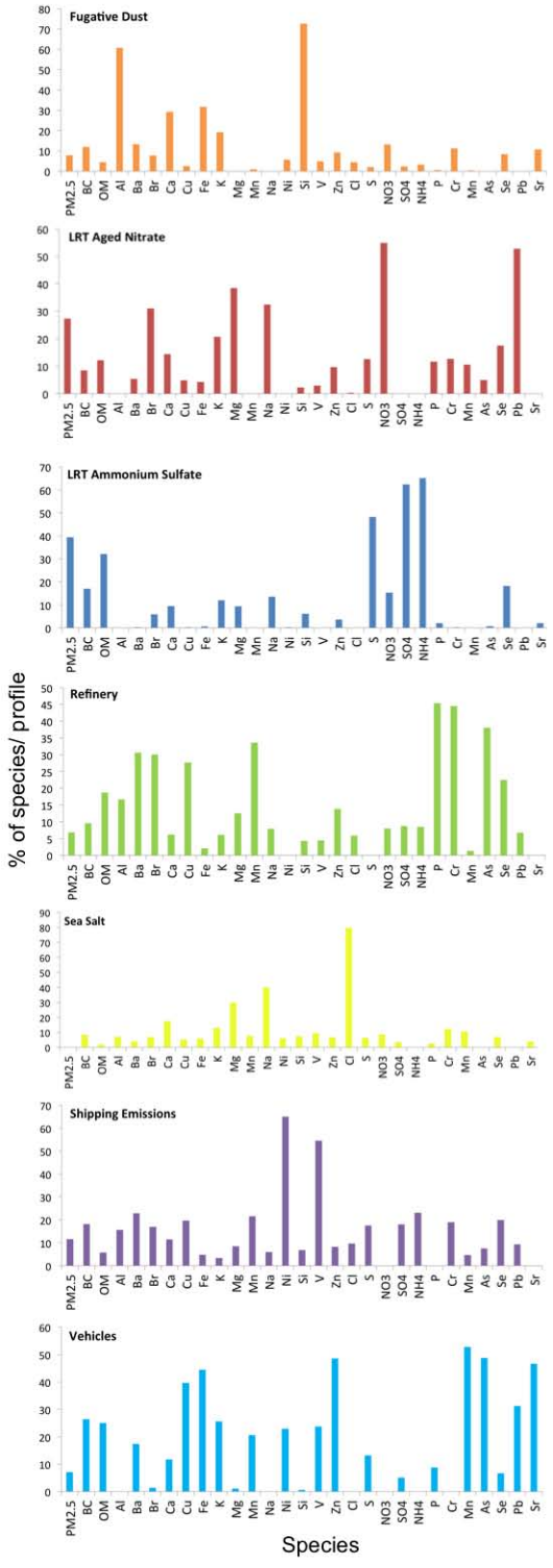

Fig. 8. Source profiles for the seven PMF factors.

a time series of the six contributing sources to $PM_{2.5}$ mass estimated using PMF during BORTAS-B.

Figure 10 shows the local wind directional dependence of the $PM_{2.5}$ source contributions estimated by PMF. Ship emission $PM_{2.5}$ source contribution aligns with the cruise ship terminal, harbour shipping lane and naval base, with little ship emission contribution directly to WNW, which is in the opposite direction to the harbour. Figure 10 confirms that ship emissions were correctly allocated to the PMF factor profile. Figure 9 shows that between 13 July and 16 July the main contributing $PM_{2.5}$ source were vehicles, which can be explained by the N and NW wind directions (Table 2) aligned with the highways directly upwind of the DGS. The fugitive dust source is most probably associated with immediate local surficial material re-suspension (Harrison et al., 2011). From Fig. 10, it was found that the fugitive dust was associated with a westerly wind direction. This wind direction is coincident with the major street landscaping that occurred directly below the western side of the DGS throughout BORTAS-B. It was found that the refinery source does not appear to have a strong local wind directional dependence. The refinery is on the other side of Halifax harbour so that the local wind direction is less appropriate than for more immediate local sources such as vehicles and fugitive dust. Air mass back trajectory analysis did not yield any further insight into wind direction dependence for the refinery source. Marine inversions and the complexity of the harbour and city topography that lay between the refinery and the DGS may have perturbed any wind directional dependence for this source.

Figure 11 shows the PMF source contribution for LRTP and LRTPMM associated with the SW and W air mass back trajectories. The back trajectories associated with the days with high loadings of LRTP have all passed over eastern Canada or the NE US (Fig. 11). This is a known large upwind source of sulphur to the region (Jeong et al., 2011). The days with high loadings of LRTPMM (Fig. 11) have more variability. While the trajectories generally come from the W, several of the back trajectories have primarily been over the ocean for most of the 48 h. The presence of Na and the loss of Cl associated with the LRTPMM source suggest continental acidic aerosol outflow mixing with marine aerosol en route to Halifax (Holzinger et al., 2007; Leaitch et al., 1996).

Figure 12 shows the average mass and (percentage) contribution from the six sources estimated by PMF during BORTAS-B. The refinery contribution of $0.081\,\mu g\,m^{-3}$ (2.2 %) during BORTAS-B is somewhat lower than $0.3\,\mu g\,m^{-3}$ (3.5 %) as obtained by PMF conducted by Jeong et al. (2011) (Jeong-PMF). The comparison for the BORTAS-B PMF vehicles with Jeong-PMF vehicle $PM_{2.5}$ mass contribution was $0.49\,\mu g\,m^{-3}$ (13.2 %) and $1.0\,\mu g\,m^{-3}$ (14.2 %) respectively, which is very similar in terms of % contribution but half the $PM_{2.5}$ mass seen during BORTAS-B. Regarding the comparison between the BORTAS-B PMF and Jeong-PMF for the ship emission was $0.13\,\mu g\,m^{-3}$ (3.4 %) and $0.6\,\mu g\,m^{-3}$ (9.1 %) respectively,

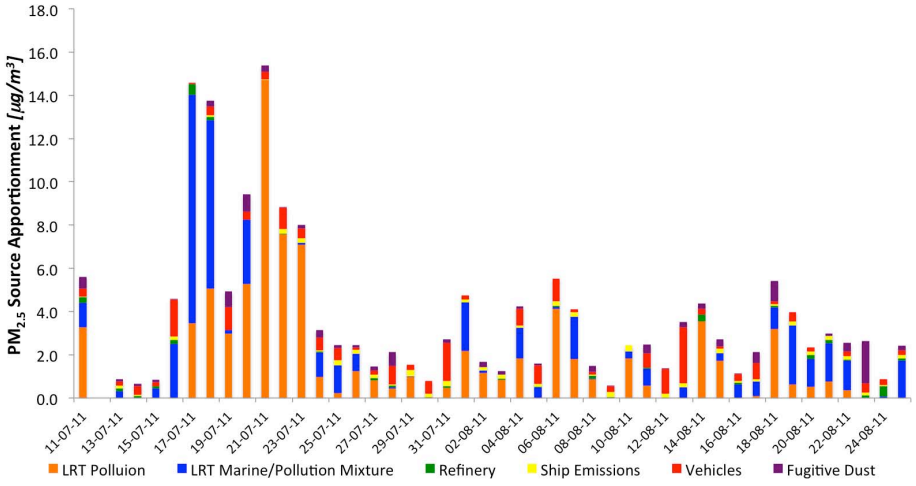

Fig. 9. Time series of $PM_{2.5}$ source apportionment based upon PMF output

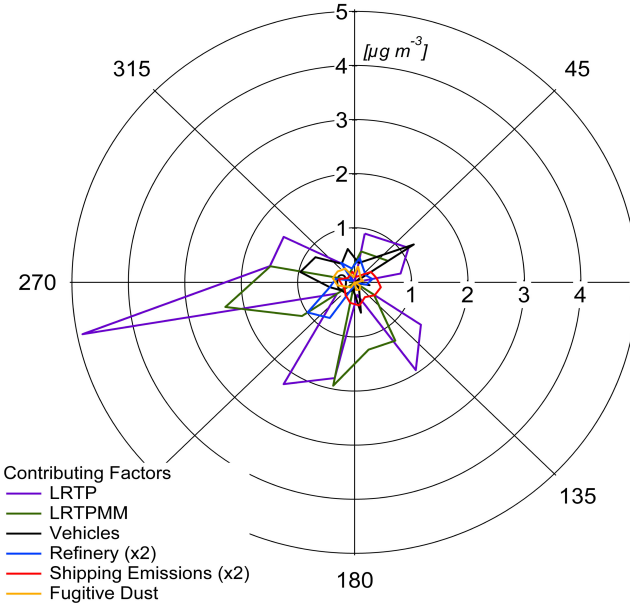

Fig. 10. Source contribution rose.

showing a 4.6 times mass reduction and 3 times reduction in % contribution between the previous PMF study conducted on 2006–2008 data and the BORTAS-B study. This could be due to the reduction in the sulphur content (3.5 % to 1 %) of HFO used in ships in the intervening period between these two studies, which, coincidentally, is the same ratio of sulphur reduction in HFO as the $PM_{2.5}$ mass reduction seen in the BORTAS-B study. The comparison between BORTAS-B PMF and Jeong-PMF fugitive dust is $0.23\,\mu g\,m^{-3}$ (6.3 %) and $0.3\,\mu g\,m^{-3}$ (3.8 %) respectively. Both are similar in magnitude for $PM_{2.5}$ mass but with a 39 % greater contribution to $PM_{2.5}$ during BORTAS-B. The fugitive dust contribution during BORTAS-B can be explained by street landscaping and exterior building restoration work that occurred during BORTAS-B. The comparison between BORTAS-B PMF and Jeong-PMF for the LRTP was $1.75\,\mu g\,m^{-3}$ (47 %) and $2.6\,\mu g\,m^{-3}$ (37.3 %), which are similar in magnitude – providing confidence in the BORTAS-B PMF results. The comparison between BORTAS-B PMF LRTPMM and Jeong-PMF LRTPMM, Jeong et al. (2011) estimated that secondary NO_3 aerosol in Halifax was $1.0\,\mu g\,m^{-3}$ (27.9 %) and $0.7\,\mu g\,m^{-3}$ (9.3 %), which is again similar in mass contribution to BORTAS-B but roughly three times the % contribution when compared to the Jeong-PMF results. The factor associated with "unaltered" sea salt was identified in the BORTAS-B samples, but there was too little mass for PMF to apportion, although aged marine aerosol did contribute to the LRTPMM source. The Jeong-PMF reported a sea salt contribution of $1.3\,\mu g\,m^{-3}$ (18.3 %) contribution to $PM_{2.5}$ mass in Halifax; however this was an average over two years and included all seasons (Jeong et al., 2011).

Linear regression of the PMF model versus observed $PM_{2.5}$ mass yielded a slope of 0.87, intercept of 1.24 and $R^2 = 0.87$. The PMF model bias = 0.17 and the RSME = $1.5\,\mu g\,m^{-3}$, showing that the PMF model skill was high.

5 Conclusion

The PMF model was used to determine six major sources contributing to the $PM_{2.5}$ mass sampled during the BORTAS-B study. Although other BORTAS-B-related observations (Palmer et al., 2013) showed that transient boreal wildfire smoke plumes did pass over and impact the surface in Halifax, there was insufficient mass for PMF to apportion. However, this study does provide valuable new insight into the major local and distant sources contributing to surface $PM_{2.5}$ mass at the DGS during BORTAS-B.

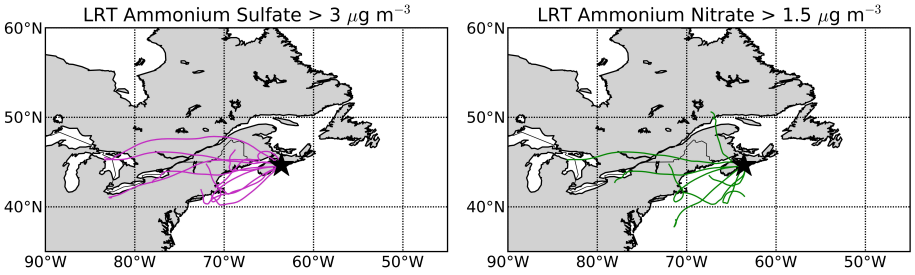

Fig. 11. Back trajectories associated with the highest values of each PMF cluster.

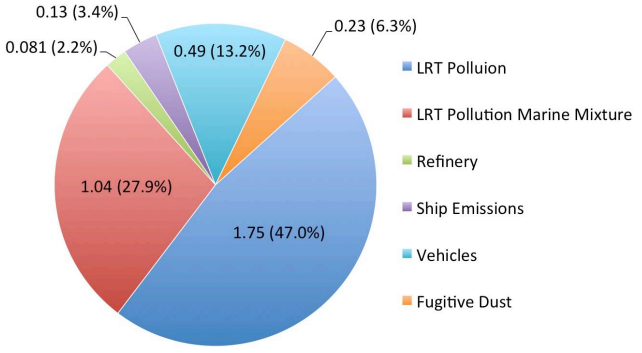

Fig. 12. Average mass concentration ($\mu g\,m^{-3}$) of attributed sources and percentage source contributions over the 45 days of sampling.

It was shown that the dominant source contribution to summertime $PM_{2.5}$ mass in Halifax was from LRT pollution with a contribution from aged marine aerosol (75 %) coincident with SW airflow. This is consistent with the conventional wisdom that Nova Scotia is the "tail pipe of North America". Comparison of the PMF total $PM_{2.5}$ mass with the observed total $PM_{2.5}$ mass over the sampling period showed good agreement ($R^2 = 0.87$, bias = 0.17 and RSME = 1.5 $\mu g\,m^{-3}$), demonstrating the PMF receptor model performed well. The study highlights the utility of using air mass back trajectories coupled with local wind direction dependence to help identify the source of $PM_{2.5}$. The techniques used in this study show considerable promise for further application to other sites and to identify other source categories of $PM_{2.5}$. In addition, the individual $PM_{2.5}$ species and source apportionment data provide valuable comparative data that can be used to interpret other collocated ground-based measurements of atmospheric composition made at the BORTAS-B Dalhousie Ground Station.

Acknowledgements. The authors are grateful to Paul Palmer (University of Edinburgh) for funding project consumables via his Philip Leverhulme Prize. The authors would like to thank Health Canada for the loan of the Magee black carbon Aethalometer, Thermo ChemComb samplers, filter weighing and XRF analysis. Many thanks to CD-NOVA for the loan of the Thermo Partisol 2025-Dichotomous sampler. Gratitude to Heather Daurie, Department of Civil and Resources Engineering, Dalhousie University, for analysing the water-soluble metals species. The authors acknowledge the support of Nova Scotia Environment, Air Quality Section, for the provision of comparative air pollution data and general support and advice.

Edited by: S. Matthiesen

References

Babu, S. S. and Moorthy, K. K.: Aerosol black carbon over a tropical coastal station in India, Geophys. Res. Lett., 29, 13-11–13-14, 2002.

Bari, M. A., Baumbach, G., Kuch, B., and Scheffknecht, G.: Wood smoke as a source of particle-phase organic compounds in residential areas, Atmos. Environ., 43, 4722–4732, 2009.

Bergauff, M. A., Ward, T. J., Noonan, C. W., Migliaccio, C. T., Simpson, C. D., Evanoski, A. R., and Palmer, C. P.: Urinary levoglucosan as a biomarker of wood smoke: Results of human exposure studies, J. Expo. Sci. Env. Epid., 20, 385–392, 2010.

Brown, S. G., Frankel, A., and Hafner, H. R.: Source apportionment of VOCs in the Los Angeles area using positive matrix factorization, Atmos. Environ., 41, 227–237, 2007.

Bukowiecki, N., Lienemann, P., Hill, M., Furger, M., Richard, A., Amato, F., Prévôt, A. S. H., Baltensperger, U., Buchmann, B., and Gehrig, R.: PM_{10} emission factors for non-exhaust particles generated by road traffic in an urban street canyon and along a freeway in Switzerland, Atmos. Environ., 44, 2330–2340, 2010.

Calvert, J. G., Lazrus, A., Kok, G. L., Heikes, B. G., Walega, J. G., Lind, J., and C. A. Cantrell: Chemical mechanisms of acid generation in the troposphere, Nature, 317, 27–35, 1985.

Chen, F., Dimmick, F., Williams, R., and Baldauf, R.: Particulate Matter Concentration Measurements from Near Road Studies (NRS) in Raleigh, North Carolina, 17th Annual Conference of the International Society for Exposure Analysis, Durham, Research Triangle Park, North Carolina, 2007.

Chow, J. C., Watson, J. G., Kuhns, H., Etyemezian, V., Lowenthal, D. H., Crow, D., Kohl, S. D., Engelbrecht, J. P., and Green, M. C.: Source profiles for industrial, mobile, and area sources in the Big Bend Regional Aerosol Visibility and Observational study, Chemosphere, 54, 185–208, 2004.

Dabek-Zlotorzynska, E., Dann, T. F., Martinelango, P. K., Celo, V., Brook, J. F., Mathieu, D., Ding, L., and Austin, C. C.: Canadian National Air Pollution Surveillance (NAPS) $PM_{2.5}$ speciation program: Methodology and $PM_{2.5}$ chemical composition for the years 2003–2008, Atmos. Environ., 45, 673–686, 2011.

Draxler, R. R. and Rolph, G. D.: HYSPLIT (HYbrid Single-Particle Lagrangian Integrated Trajectory) Model access via NOAA ARL READY Website, NOAA Air Resources Laboratory, Silver Spring, MD, 2012.

Finlayson-Pitts, B. J. and Pitts, J. N.: Chemistry of the Upper and Lower Atmosphere, Academic Press, Academic Press, ISBN 0-12-257060-x, 1999.

Gibson, M. D., Heal, M. R., Bache, D. H., Hursthouse, A. S., Beverland, I. J., Craig, S. E., Clark, C. F., Jackson, M. H., Guernsey, J. R., and Jones, C.: Using Mass Reconstruction along a Four-Site Transect as a method to interpret PM_{10} in West-Central Scotland, United Kingdom, JAPCA J. Air Waste Ma., 59, 1429–1436, 2009.

Gibson, M. D., Heal, M. R., Li, Z., Kuchta, J., King, G. H., Hayes, A., and Lambert, S.: The spatial and seasonal variation of nitrogen dioxide and sulfur dioxide in Cape Breton Highlands National Park, Canada, and the association with lichen abundance, Atmos. Environ., 64, 303–311, 2013.

Gietl, J. K., Lawrence, R., Thorpe, A. J., and Harrison, R. M.: Identification of brake wear particles and derivation of a quantitative tracer for brake dust at a major road, Atmos. Environ., 44, 141–146, 2010.

Gugamsetty, B., Wei, H., Liu, C. N., Awasthi, A., Hsu, S. C., Tsai, C. J., Roam, G. D., Wu, Y. C., and Chen, C. F.: Source Characterization and Apportionment of PM_{10}, $PM_{2.5}$ and $PM_{0.1}$ by Using Positive Matrix Factorization, Aerosol Air Qual. Res., 12, 476–491, 2012.

Hansen, A. D. A.: The Aethalometer, Magee Scientific Company, Berkeley, California, USA, 1–209, 2005.

Harrison, R. M., Beddows, D. C. S., and Dall'Osto, M.: PMF Analysis of Wide-Range Particle Size Spectra Collected on a Major Highway, Environ. Sci. Technol., 45, 5522–5528, 2011.

Hennigan, C. J., Miracolo, M. A., Engelhart, G. J., May, A. A., Presto, A. A., Lee, T., Sullivan, A. P., McMeeking, G. R., Coe, H., Wold, C. E., Hao, W.-M., Gilman, J. B., Kuster, W. C., de Gouw, J., Schichtel, B. A., J. L. Collett Jr., Kreidenweis, S. M., and Robinson, A. L.: Chemical and physical transformations of organic aerosol from the photo-oxidation of open biomass burning emissions in an environmental chamber, Atmos. Chem. Phys., 11, 7669–7686, doi:10.5194/acp-11-7669-2011, 2011.

Hobbs, P. V., Garrett, T. J., Ferek, R. J., S.R., S., Hegg, D. A., Frick, G. M., Hoppel, W. A., Gasparovic, R. F., Russell, L. M., Johnson, D. W., O'Dowd, C., Durkee, P. A., Nielson, K. E., and Innis, G.: Emissions from ships with respect to their effects on clouds, J. Atmos. Sci., 57, 2570–2590, 2000.

Holzinger, R., Millet, D. B., Williams, B., Lee, A., Kreisberg, N., Hering, S. V., Jimenez, J., Allan, J. D., Worsnop, D. R., and Goldstein, A. H.: Emission, oxidation, and secondary organic aerosol formation of volatile organic compounds as observed at Chebogue Point, Nova Scotia, J. Geophys. Res., 112, D10S24, doi:10.1029/2006jd007599, 2007.

Hopke, P. K.: An introduction to Receptor Modeling, Chemometr. Intell. Lab., 10, 21–43, 1991.

Huang, X., Olmez, I., Aras, N. K., and Gordon, G. E.: Emissions of trace elements from motor vehicles: Potential marker elements and source composition profile, Atmos. Environ., 28, 1385–1391, 1994.

Isakson, J., Persson, T. A., and Lindgren, E. S.: Identification and assessment of ship emissions and their effects in the harbour of Goteborg, Sweden, Atmos. Environ., 35, 3659–3666, 2001.

Jaeckels, J. M., Bae, M.-S., and Schauer, J. J.: Positive Matrix Factorization (PMF) Analysis of Molecular Marker Measurements to Quantify the Sources of Organic Aerosols, Environ. Sci. Technol., 41, 5763–5769, 2007.

Jeong, C.-H., Evans, G. J., Dann, T., Graham, M., Herod, D., Dabek-Zlotorzynska, E., Mathieu, D., Ding, L., and Wang, D.: Influence of biomass burning on wintertime fine particulate matter: Source contribution at a valley site in rural British Columbia, Atmos. Environ., 42, 3684–3699, 2008.

Jeong, C.-H., McGuire, M. L., Herod, D., Dann, T., Dabek–Zlotorzynska, E., Wang, D., Ding, L., Celo, V., Mathieu, D., and Evans, G.: Receptor model based identification of $PM_{2.5}$ sources in Canadian cities, Atmospheric Pollution Research, 2, 158–171, 2011.

Lack, D. A. and Corbett, J. J.: Black carbon from ships: a review of the effects of ship speed, fuel quality and exhaust gas scrubbing, Atmos. Chem. Phys., 12, 3985–4000, doi:10.5194/acp-12-3985-2012, 2012.

Lack, D. A., Cappa, C. D., Langridge, J., Bahreini, R., Buffaloe, G., Brock, C., Cerully, K., Coffman, D., Hayden, K., Holloway, J., Lerner, B., Massoli, P., Li, S.-M., McLaren, R., Middlebrook, A. M., Moore, R., Nenes, A., Nuaanan, I., Onasch, T. B., Peischl, J., Perring, A., Quinn, P. K., Ryerson, T., Schwartz, J. P., Spackman, R., Wofsy, S. C., Worsnop, D., Xiang, B., and Williams, E.: Impact of Fuel Quality Regulation and Speed Reductions on Shipping Emissions: Implications for Climate and Air Quality, Environ. Sci. Technol., 45, 9052–9060, 2011.

Larson, T., Gould, T., Simpson, C., Liu, L. J., Claiborn, C., and Lewtas, J.: Source Apportionment of Indoor, Outdoor, and Personal $PM_{2.5}$ in Seattle, Washington, Using Positive Matrix Factorization, JAPCA J. Air Waste Ma., 54, 1175–1187, 2004.

Laupsa, H., Denby, B., Larssen, S., and Schaug, J.: Source apportionment of particulate matter ($PM_{2.5}$) in an urban area using dispersion, receptor and inverse modelling, Atmos. Environ., 43, 4733–4744, 2009.

Lawless, P. A., Rodes, C. E., and Ensor, D. S.: "Multiwavelength absorbance of filter deposits for determination of environmental tobacco smoke and black carbon", Atmos. Environ., 38, 3373–3383, 2004.

Leaitch, W. R., Banic, C. M., Isaac, G. A., Couture, M. D., Liu, P. S. K., Gultepe, I., Li, M. M., Klienman, L., Daum, P. H., and MacPherson, J. I.: Physical and chemical observations in marine stratus during the 1993 North Atlantic Regional Experiment: Factors controlling cloud droplet number concentrations, J. Geophys. Res., 101, 29123–29135, 1996.

Liu, P. S. K., Deng, R., Smith, K. A., Williams, L. R., Jayne, J. T., Canagaratna, M. R., Moore, K., Onasch, T. B., Worsnop, D. R., and Deshler, T.: Transmission Efficiency of an Aerodynamic Focusing Lens System: Comparison of Model Calculations and Laboratory Measurements for the Aerodyne Aerosol Mass Spectrometer, Aerosol Sci. Tech., 41, 721–733, 2007.

Martello, D. V., Pekneya, N. J., Anderson, R. R., Davidson, C. I., Hopke, P. K., Kim, E., Christensen, W. F., Mangelson, N. F., and Eatough, D. J.: Apportionment of Ambient Primary and Secondary Fine Particulate Matter at the Pittsburgh National Energy Laboratory Particulate Matter Characterization Site Using Positive Matrix Factorization and a Potential Source Contributions Function Analysis, JAPCA J. Air Waste Ma., 58, 357–368, 2008.

Maykut, N. N., Lewtas, J., Kim, E., and Larson, T. V.: Source Apportionment of $PM_{2.5}$ at an Urban IMPROVE Site in Seattle, Washington, Environ. Sci. Technol., 37, 5135–5142, 2003.

Ng, N. L., Herndon, S. C., Trimborn, A., Canagaratna, M. R., Croteau, P. L., Onasch, T. B., Sueper, D., Worsnop, D. R., Zhang, Q., Sun, Y. L., and Jayne, J. T.: An Aerosol Chemical Speciation Monitor (ACSM) for Routine Monitoring of the Composition and Mass Concentrations of Ambient Aerosol, Aerosol Sci. Tech., 45, 780–794, 2011.

Olajire, A. A. and Ayodele, E. T.: Contamination of roadside soil and grass with heavy metals, Environ. Int., 23, 91–101, 1997.

Paatero, P.: Least squares formulation of robust non-negative factor analysis, Chemometr. Intell. Lab., 37, 23–35, 1997.

Paatero, P. and Trapper, U.: Positive matrix factorization: a non-negative factor model with optimal utilization of error estimates of data values, Environmetrics, 5, 111–126, 1994.

Palmer, P. I., Parrington, M., Lee, J. D., Lewis, A. C., Rickard, A. R., Bernath, P. F., Duck, T. J., Waugh, D. L., Tarasick, D. W., Andrews, S., Aruffo, E., Bailey, L. J., Barrett, E., Bauguitte, S. J.-B., Curry, K. R., Di Carlo, P., Chisholm, L., Dan, L., Forster, G., Franklin, J. E., Gibson, M. D., Griffin, D., Helmig, D., Hopkins, J. R., Hopper, J. T., Jenkin, M. E., Kindred, D., Kliever, J., Le Breton, M., Matthiesen, S., Maurice, M., Moller, S., Moore, D. P., Oram, D. E., O'Shea, S. J., Owen, R. C., Pagniello, C. M. L. S., Pawson, S., Percival, C. J., Pierce, J. R., Punjabi, S., Purvis, R. M., Remedios, J. J., Rotermund, K. M., Sakamoto, K. M., da Silva, A. M., Strawbridge, K. B., Strong, K., Taylor, J., Trigwell, R., Tereszchuk, K. A., Walker, K. A., Weaver, D., Whaley, C., and Young, J. C.: Quantifying the impact of BORReal forest fires on Tropospheric oxidants over the Atlantic using Aircraft and Satellites (BORTAS) experiment: design, execution and science overview, Atmos. Chem. Phys., 13, 6239–6261, doi:10.5194/acp-13-6239-2013, 2013.

Parrington, M., Palmer, P. I., Henze, D. K., Tarasick, D. W., Hyer, E. J., Owen, R. C., Helmig, D., Clerbaux, C., Bowman, K. W., Deeter, M. N., Barratt, E. M., Coheur, P.-F., Hurtmans, D., Jiang, Z., George, M., and Worden, J. R.: The influence of boreal biomass burning emissions on the distribution of tropospheric ozone over North America and the North Atlantic during 2010, Atmos. Chem. Phys., 12, 2077–2098, doi:10.5194/acp-12-2077-2012, 2012.

Rolph, G. D.: Real-time Environmental Applications and Display sYstem (READY), NOAA Air Resources Laboratory, Silver Spring, MD, 2012.

Tereszchuk, K. A., González Abad, G., Clerbaux, C., Hadji-Lazaro, J., Hurtmans, D., Coheur, P.-F., and Bernath, P. F.: ACE-FTS observations of pyrogenic trace species in boreal biomass burning plumes during BORTAS, Atmos. Chem. Phys., 13, 4529–4541, doi:10.5194/acp-13-4529-2013, 2013.

USEPA: $PM_{2.5}$ Mass Weighing Laboratory Standard Operating Procedures for the Performance Evaluation Program, Quality Assurance Guidance Document Method Compendium, 1–165, 1998.

Ward, T. J., Trost, B., Conner, J., Flanagan, J., and Jayanty, R. K. M.: $PM_{2.5}$ source Apportionment in a Subarctic Airshed – Fairbanks, Alaska, Aerosol Air Qual. Res., 12, 536–543, 2012.

Yin, J. and Harrison, R. M.: Pragmatic mass closure study for $PM_{1.0}$, $PM_{2.5}$ and PM_{10} at roadside, urban background and rural sites, Atmos. Environ., 42, 980–988, 2008.

Zhao, M., Zhang, Y., Ma, W., Fu, Q., Yang, X., Li, C., Zhou, B., Yu, Q., and Chen, L.: Characteristics and ship traffic source identification of air pollutants in China's largest port, Atmos. Environ., 64, 277–286, 2013.